Hydrodynamic diffusion and mass transfer across a sheared suspension of neutrally buoyant spheres

Luying Wang, Donald L. Koch, Xiaolong Yin, and Claude Cohen

View Online   Export Citation

ARTICLES YOU MAY BE INTERESTED IN

Physics of Fluids GALLERY OF COVERS
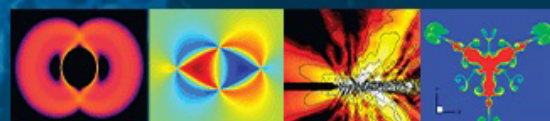
AIP Publishing

Hydrodynamic diffusion and mass transfer across a sheared suspension of neutrally buoyant spheres

Luying Wang, Donald L. Koch, Xiaolong Yin, and Claude Cohen

School of Chemical and Biomolecular Engineering, Cornell University, Ithaca, New York 14853, USA

We present experimental, theoretical, and numerical simulation studies of the transport of fluid-phase tracer molecules from one wall to the opposite wall bounding a sheared suspension of neutrally buoyant solid particles. The experiments use a standard electrochemical method in which the mass transfer rate is determined from the current resulting from a dilute concentration of ions undergoing redox reactions at the walls in a solution of excess nonreacting ions that screen the electric field in the suspension. The simulations use a lattice-Boltzmann method to determine the fluid velocity and solid particle motion and a Brownian tracer algorithm to determine the chemical tracer mass transfer. The mass transport across the bulk of the suspension is driven by hydrodynamic diffusion, an apparent diffusive motion of tracers caused by the chaotic fluid velocity disturbances induced by suspended particles. As a result the dimensionless rate of mass transfer (or Sherwood number) is a nearly linear function of the dimensionless shear rate (Peclet number) at moderate values of the Peclet number. At higher Peclet numbers, the Sherwood number grows more slowly due to the mass transport resistance caused by a molecular-diffusion boundary layer near the solid walls. Fluid inertia enhances the rate of mass transfer in suspensions with particle Reynolds numbers in the range of 0.5–7. © *2009 American Institute of Physics.* [DOI: 10.1063/1.3098446]

I. INTRODUCTION

Transport of heat and mass into a suspension of particles is important in slurry reactors where reactions that consume and/or generate chemical species and heat occur in catalyst particles that are suspended in a flowing fluid. Mass transport also provides for the supply of nutrients and oxygen and removal of wastes including CO_2 from cell suspensions. These processes involve two coupled mass/heat transfer processes, the transport from the flow boundaries into the suspension and the interphase transport from the fluid to the particles. In the present investigation, we will isolate the boundary-suspension transport process by considering model suspensions where the chemical tracers do not penetrate the particulate phase. We will consider laminar shearing flows of continuum suspensions where the convective transport is dominated by the fluid velocity disturbances induced by the suspended particles as may occur when the 100 μm−2 mm size of the flow conduits is large compared with the particle size but small enough to maintain laminar flow. Examples would include transport to particles synthesized in microreactors[1] and to cells in hollow-fiber artificial lung devices.[2]

We will consider a suspension of neutrally buoyant, non-Brownian solid particles sheared between two parallel walls. The walls are planar in the simulation and are cylinders of a small-gap Couette cell in the experiments. Tracers are produced at one wall, transported through the fluid phase, and are consumed at the opposite wall. The solid particles are impermeable to the fluid-phase tracers, and there are no significant chemical kinetic limitations to production and consumption of the chemical species at the walls.

The rate of mass transfer can be expressed in dimensionless form as the Sherwood number, $Sh = hH/D$, where h $= Q/Ac_0$ is the mass transfer coefficient, Q is the mass flux, A is the area of each wall, c_0 is the concentration driving force, H is the gap between the walls, and D is the molecular diffusivity of the tracers. The rate of mass transfer is primarily dependent on the Peclet number, $Pe = \Gamma a^2/D$, where Γ is the mean shear rate (ΓH being the relative velocity of the two walls) and a is the radius of the solid suspended particles. This Peclet number characterizes the relative importance of the microconvective flow produced by the particles and molecular diffusion in causing transport of a fluid tracer. Here, a is the characteristic length scale of the fluid velocity fluctuations produced by the particles and Γa is the characteristic magnitude of these velocity disturbances. The particle-scale Reynolds number $Re = \Gamma a^2/\nu$ can also influence the rate of mass transfer by virtue of the effects that it has on the particle-induced velocity disturbances. Here, ν is the kinematic viscosity of the fluid. One can also define a Reynolds number $Re_H = \Gamma H^2/\nu$ based on the gap H between the walls. The sole importance of this parameter in the present study is that it has been maintained at a sufficiently small value throughout the study so that the fluid-phase flow will be laminar in the absence of the particles. Under these conditions we do not expect Re_H to affect the rate of mass transfer.

In the absence of the particles, the simple shear flow between two walls has streamlines that are perpendicular to the direction of the imposed concentration gradient. As a result, convective mass transfer would be absent and the mass transfer across the fluid-filled gap would occur purely by molecular diffusion. This situation leads to a Sherwood number of 1. Neutrally buoyant particles tend to translate and rotate with the fluid motion. However, they resist the straining motion of the shear flow and thereby produce fluid velocity disturbances. In a moderately concentrated, disor-

dered suspension, these fluid velocity disturbances are chaotic. A fluid-phase tracer may be expected to have a diffusive motion resulting from this chaotic flow on time scales larger than the $O(1/\Gamma)$ time required for the solid particle configuration surrounding the fluid particle to change. This phenomenon is referred to as hydrodynamic diffusion. If the Reynolds number Re based on the solid particle radius a is very small and the molecular diffusion of the fluid tracer is negligible, then the hydrodynamic diffusivity D_H can only depend on the shear rate Γ, solid particle radius a, and the volume fraction of the solid particles ϕ. Dimensional analysis then implies that $D_H = \Gamma a^2 D_H^*$, where D_H^* is a dimensionless function of ϕ. When the Peclet number is much larger than 1, $D_H \gg D$, and hydrodynamic diffusion would be expected to greatly enhance the rate of mass transfer in the bulk of a sheared suspension. Hydrodynamic diffusion of solid particles due to their interactions with other solid particles in shear flows has been widely studied in experiments, numerical simulations, and theories.[3–10] Relatively little is known about the hydrodynamic diffusion of chemical tracers in sheared suspensions and that is the focus of this paper.

Although hydrodynamic diffusion may lead to rapid transport of a tracer across the bulk of a particle suspension or porous medium, Koch[11] pointed out that the hydrodynamic diffusivity must decrease near a solid boundary to the suspension as a result of the no-slip boundary condition on the wall. This leads to a boundary layer near the wall in which molecular diffusion plays an important role even if $Pe \gg 1$. Koch evaluated the hydrodynamic diffusivity as a function of the distance from the wall in a bounded, dilute, fixed fibrous medium. For the case of a neutrally buoyant suspension of particles sheared between two planar walls, Koch presented only a scaling analysis. In the present study we will obtain quantitative predictions for the mass transfer across a bounded sheared particle suspension using numerical simulations to determine the dimensionless hydrodynamic diffusivity D_H^* and the boundary layer resistance to mass transfer.

Our numerical simulations make use of a lattice-Boltzmann method for simulation of particle suspensions developed by Ladd.[12–14] The simulation considers a suspension of solid particles in a fluid bounded by two planar walls separated by a distance H and translating with velocities $\pm \Gamma H/2$. The fluid motion is evaluated on a spatially uniform grid using the lattice-Boltzmann method and the evolution of the particle configuration is determined by solving Newton's equations for their motion subject to the hydrodynamic forces. Lattice-Boltzmann provides an efficient simulation of the Navier–Stokes equations in the range of particle Reynolds numbers $Re = 0.1 - 10$ considered here. The mass transfer is evaluated by considering many fluid-phase tracers. These tracers are convected by a fluid velocity obtained by interpolating the lattice-Boltzmann mean velocity field, and they undergo random Brownian displacements to model their molecular diffusion. If the Brownian motion causes a tracer to cross the boundary of a solid particle, it has a specular reflection to approximate the no flux condition at the particle surface. Two species of tracers are considered, which undergo reactions at the two adjacent walls producing equal

and opposite driving forces for the transport of the two species.

In our experimental study, we measure the current resulting from the transport of two ionic species, ferricyanide and ferrocyanide, that undergo redox reactions with negligible chemical kinetic limitations at the nickel coated cylinders of a small-gap cylindrical Couette cell. A large concentration of an electrolyte (sodium hydroxide) that does not react at the electrodes screens the electric field so that the current is determined by the convection-diffusion of the ions within the suspension. The suspended solid particles are monodisperse, impermeable polystyrene spheres whose density is matched with that of the suspending fluid.

In the simulations, it is straightforward to vary independently the primary dimensionless parameters, Pe, H/a, and Re, that influence the rate of mass transfer. From the simulations we develop an analytical model describing $Sh(Pe, Re, H/a)$. In experiments, such as those performed here, where one uses a single fluid system, the Schmidt number $Sc = \nu/D$ is held fixed. Thus, $Pe = Sc\, Re$ in the experiments and the Reynolds and Peclet numbers are not varied independently. Nonetheless the experiments provide a partial validation of the theory. The theory also provides a means of distinguishing effects of convection and fluid inertia, both of which increase with increasing Γ and provide a richer understanding of the experimental results.

The two previous experimental investigations that bear the closest resemblance to our study are those of Wang and Keller[15] and Sohn and Chen.[16] Wang and Keller used the same electrochemical technique employed in our work. However, their suspended particles were red-blood cells. Thus, the particles had a nonspherical shape (disklike with an aspect ratio—thickness to diameter) of about 0.25. In addition, cell deformation and nonhydrodynamic interactions among the cells may have influenced this study. Sohn and Chen investigated the heat transfer in a suspension of spherical particles in a viscous liquid. The primary difference between the heat and mass transfer problems is that the finite heat capacity of the particles implies that part of the heat is transferred through the particulate phase, whereas the impermeable particles do not transport the chemical tracers in our study or that of Wang and Keller. In a liquid-solid suspension such as that investigated by Sohn and Chen, the convective transports of heat by the particle and fluid phases are comparable. In contrast, the heat transfer through the bulk of a gas-solid suspension occurs predominantly through the fluctuating convective motions of the solid particles. However, even in this case the transport near the solid wall occurs through convection and diffusion in the gas phase.[17,18] Our experimental study is the first to (a) explore the influence of the ratio of the gap thickness to the particle radius, H/a; (b) isolate fluid-phase transport in a system with ideal hard-sphere particles; and (c) consider effects of finite Re on transport into a liquid-solid suspension.

We describe the experimental and numerical methods used in the present study in Secs. II and III, respectively. The results of the experiments and simulations are presented and discussed in light of a simple theoretical model in Sec. IV.

II. EXPERIMENTAL METHODS

Our mass transfer measurements were made using a standard electrochemical technique that has been widely used to study transport to solid surfaces by the coupled effects of convection and molecular diffusion.[15,19–23] Wang and Keller[15] employed this method to determine the mass transfer across a Couette cell containing a suspension of red-blood cells. In this method, the mass transfer rate is determined from the limiting current, i.e., the electrical current that passes through the suspension in the limit of high voltage difference across the suspension. The current is carried by a pair of electrolytes which undergo redox reactions at the electrode surfaces. The electrode surfaces in our flow measurements are the inner and outer cylinders of a Couette cell. The ions carrying the current and the electrode surface are chosen so that the surface reaction is sufficiently fast for convective-diffusive mass transfer across the suspension to be the rate limiting step. We adopted the classic choice of ferricyanide $Fe(CN)_6^{-3}$ and ferrocyanide $Fe(CN)_6^{-4}$ ions reacting at nickel-plated electrode surfaces. To prevent oxidation reactions which can reduce the current, we polished the electrodes and conducted the experiments under a nitrogen atmosphere. To assure that ion transport by convection and diffusion dominates over that due to electrical migration, an excess of an electrolyte that screens the electric field but does not react at the surfaces is added. The inert electrolyte in our study is sodium hydroxide (NaOH).

In the absence of surface chemical kinetic limitations, the concentration of the ions at the electrode surfaces satisfies an equilibrium condition that depends on the electrical potential.[19] For sufficiently large potential differences, this equilibrium condition yields a concentration drop across the suspension for the ionic species with the lower diffusivity (ferrocyanide) that is equal to c_0, the sum of the initial concentrations of the two redox ion species. The flux of ions per unit area, Q, is related to the limiting current i_L for high potential difference by

$$Q = \frac{i_L}{nFA}, \tag{1}$$

where F is Faraday's constant, n is the number of electrons transferred in the surface reaction ($n=1$ for ferricyanide and ferrocyanide), and A is the surface area of each electrode. The mass transfer coefficient h, defined as the mass flux per unit area divided by the concentration difference across the suspension, is

$$h = \frac{Q}{c_0}. \tag{2}$$

The dimensionless mass transfer rate or Sherwood number Sh is then

$$\text{Sh} \equiv \frac{hH}{D} = \frac{i_L H}{nAc_0 FD}, \tag{3}$$

where D is the molecular diffusivity of the less diffusive ion. For our system ferrocyanide has a diffusivity that is about 10% smaller than ferricyanide.[24] In a pure fluid at rest, Sh=1 and Eq. (3) may be used in conjunction with measure-ments of i_L to determine the molecular diffusivity D. In a flowing suspension of particles in a fluid for which D is known, Eq. (3) may be used to determine the Sherwood number.

The active surface area of the nickel electrode can be degraded by oxidation reactions if an electrical potential is applied in the presence of dissolved oxygen.[19] To prevent this, we polished the electrodes prior to conducting a set of experiments and conducted the experiments under a nitrogen atmosphere. We performed a set of preliminary measurements using a small cell consisting of two parallel nickel plates with a spacing $H \approx 2$ mm and a surface area $A \approx 600$ mm^2. The exact cell constant, A/H, for this small cell was determined by measuring the ac electrical conduction through a standard electrolyte solution. The tests performed with this cell indicated that the limiting current could be obtained for potential differences greater than or equal to 0.4 V. We were able to reproduce previously reported measurements[24] for the diffusivities of potassium ferricyanide/ferrocyanide/sodium hydroxide solutions to within 1%. It is known that the diffusivity of ferrocyanide is inversely proportional to the viscosity in sodium hydroxide solutions. By comparing the diffusivity of ferrocyanide determined in solutions with different ratios of c_{NaOH} (sodium hydroxide concentration) to c_0 (sum of ferricyanide and ferrocyanide concentration) and correcting for the dependence of the diffusivity on viscosity, we determined that a ratio $c_{NaOH}/c_0 \gtrsim 20$ is sufficient to make the contribution of electrical migration to mass transfer negligible. Our suspension experiments used a ratio $c_{NaOH}/c_0 = 600$. When the experiments were performed under standard atmospheric conditions, the current decayed significantly over a period of about 10 min. However, under a nitrogen atmosphere, a stable current could be maintained over periods of many hours that were sufficient to conduct a series of experiments exploring the parametric dependence of mass transfer on the relevant variables.

The particle-fluid mixture used in our studies consisted of a density-matched suspension of monodisperse polystyrene spheres in an aqueous solution of 1.2M sodium hydroxide, 0.001M potassium ferrocyanide, and 0.001M potassium ferricyanide. Two particle sizes were used to allow a study of the effects of H/a on the rate of mass transfer. The particle sizes were chosen so that the particle Reynolds number would span values from Stokes flow to Re=$O(1-10)$. Particles with mean radii of $a=115$ and 230 μm produced by Maxi-blast Inc. were used. Although the specifications from the manufacturer do not guarantee a narrow size distribution, we found by visual inspection under a microscope that certain batches of the particles were quite monodisperse and these batches were selected for the experiments. For example, sieving of the sample with a mean radius of 115 μm showed that it contained 98.5% by mass of particles with radii in the range of 106 μm $<a<$ 125 μm. The experiments were conducted at 22 ± 1 °C, and at this temperature the density of the solution was 1.05×10^3 kg/m^3, the kinematic viscosity ν determined by capillary viscometry was 1.2×10^{-6} m^2/s, and the diffusivity of ferrocyanide measured in the Couette cell described below was $D=5.5$

$\times 10^{-10}$ m^2/s, yielding a Schmidt number Sc$=\nu/D_f=2200$. This value of the diffusivity is consistent with measurements in the literature[24] after adjusting for the effect of the viscosity of the suspending fluid. The suspension was bubbled with nitrogen for 30 min and then sonicated and placed in a vacuum oven to remove bubbles. Thereafter the suspension was kept under a nitrogen atmosphere throughout the experiment.

The cylindrical Couette cell was designed to approximate a laminar, simple shear flow of a continuum suspension and to facilitate the electrochemical measurement. The inner diameter of the outer cylinder was $R=12$ cm, the gap thickness was $H=5$ mm, and the total height of the cylinder was 32 cm. These dimensions yield moderately large ratios of gap thickness to particle radii $H/a=22$ and 44. The large ratio of the Couette radius to gap thickness makes the curvature of the streamlines negligible on the scale of the gap and the large ratio of height to gap thickness minimizes secondary flows due to the top and bottom boundaries. In addition, the electrochemical measurements were conducted in the middle third of the cylinder to avoid the influence of end-induced secondary flows on the mass transfer. To avoid the Taylor–Couette instability, the inner cylinder was kept stationary and the outer cylinder was rotated at speeds as high as 120 rpm. This rotation speed yielded particle Reynolds and Peclet numbers as high as Re$=6.6$ and Pe$=15\,900$ for the larger particles.

For the value of $R/H=24$ used in our study, the transition to turbulence for a rotating outer cylinder occurs at Re$_H=5500$.[25] Matas *et al.*[26] observed that the onset of turbulence for low volume fraction suspensions of large particles in a pipe flow could occur at Reynolds numbers as small as about 3/4 of the critical Reynolds number for a single phase flow. The maximum Re$_H$ explored in our study was 3125, and we saw no indication of a flow transition in our mass transfer measurements.

A series of adjustments were performed to assure that the two cylinders were concentric with their axes aligned; these adjustments assured that the gap thickness was uniform to within a 200 μm tolerance. A laminar, cylindrical Couette flow in the absence of secondary flows would yield a Sherwood number equal to 1, independent of cylinder rotation rate because the streamlines would be perpendicular to the direction of the applied concentration gradient. The precautions noted above did not completely eliminate secondary flows in our experiment but the mass transfer due to secondary flows was small compared with that induced by the particles. At the highest rotation rate, the Sherwood number in a pure fluid was about 3, while the sheared particle suspensions had Sh values of about 7–20. The increase in the mass transfer rate of the pure fluid with cylinder rotation rate was gradual (approximately linear), and this suggests that the secondary flow was more likely a result of limitations in the alignment of the cylinders than a manifestation of inertial instabilities.

To facilitate the electrochemical measurement, each Couette cylinder was comprised of three sections, 10 cm tall upper and lower sections made of Plexiglas and a 12 cm tall middle section made of aluminum electroplated with a 100 μm thick nickel film. The Plexiglas sections allow viewing of the suspension to assure that sedimentation due to any slight mismatch of density is negligible. Any suspensions in which a clear layer of about 2 cm or more was observed at the top or bottom of the Couette during the period over which experiments were conducted were rejected as having an inadequate density match; this occurred in less than 5% of the experimental runs. The composite design of the Couette cylinders also assures that the electrochemical mass transfer measurement is conducted far from the top and bottom boundaries where end-induced secondary flows may occur. The electrical connection with the rotating cylinder is made using a motor brush. A hollow ring attached to the inner cylinder covers the top of the Couette gap. Nitrogen passes through the interior of this ring and flows into the space above the suspension through six holes in the ring. The gas then flows out through a narrow gap between the ring and the outer cylinder. In this way a nitrogen atmosphere is maintained above the suspension throughout the flow experiment.

The inner and outer cylinders were connected to a steady electrical power supply and an ampere meter to form a closed electrical circuit passing through the suspension. Upon changing the voltage or the rotation speed of the Couette, it typically took about 2 min for the measured current to reach a steady state. The current was then averaged over a subsequent period of 5–10 min. Measurements taken by increasing and decreasing the rotation rate in a stepwise fashion demonstrated that there was no hysteresis and the current had reached a steady state.

III. SIMULATION METHODS

We simulated the flow of a suspension of neutrally buoyant, rigid solid particles in a Newtonian fluid between two parallel flat plates separated by a distance H and moving with velocities $\pm\Gamma H/2$ and determined the convective and diffusive transport of fluid-phase tracers from one wall to the other. The motion of the fluid and solid particles was determined using the lattice-Boltzmann particle suspension method developed by Ladd.[12–14] This method solves for the velocity distribution function for a set of fluid particles which propagate across a cubic lattice. We used a 19 velocity model in which fluid particles have velocities that allow them to propagate to the nearest and next-nearest neighbors on the cubic lattice or stay at the same lattice node. At each time step, the fluid particle populations propagate and then the particles arriving at a given node undergo a collision step which relaxes the populations toward a local equilibrium in such a way that the Navier–Stokes equations are reproduced when one considers the conservation equations for the moments of the velocity distribution. Bounce-back rules for fluid particle populations encountering solid particles or solid walls enforce the no-slip boundary condition. Because the solid spherical particles move across a fixed cubic computational lattice, the boundary nodes from which the fluid particle populations are reflected form a rough boundary to the solid particle. It has been found that the accuracy of the simulation results for a variety of transport problems can be

enhanced by replacing the input radius of the sphere with an effective hydrodynamic radius chosen to make the Stokes-flow drag on a dilute cubic array of spheres match known analytical results.[27] In this study the ratios of the input and effective radius to the grid spacing were 2.72 and 2.92, respectively. These values were found to provide good resolution in a previous study of sedimenting settling suspensions with particle Reynolds numbers of 0.5–20.[28] The lattice-Boltzmann method does not resolve the lubrication force when the spacing between the particles becomes small compared with the grid spacing. However, analytical lubrication results are used to provide the correct lubrication force.[14] Although some of our simulations involve particle Reynolds numbers of the order of 1–10, viscous forces still tend to dominate in the thin lubrication gap owing to the small length scale and nearly unidirectional nature of the local flow.

The transport of the fluid-phase tracer molecules could be determined in principle by solving a continuum convection-diffusion equation for the tracer concentration c,

$$\frac{\partial c}{\partial t} + \nabla \cdot (\mathbf{v}c - D\,\nabla\,c) = 0, \tag{4}$$

subject to no flux boundary conditions on the particle surfaces and boundary conditions $c=c_0$ and $c=0$ on the planar walls that produce and consume the tracer species. Here $\mathbf{v}$ is the fluid velocity. However, the complexity of the geometry of a many-particle configuration, the time variation of this domain, and the relatively high Peclet numbers to be explored would make the computational cost of such an approach prohibitive. As an alternative, we can simulate the motion of many tracer molecules that translate in response to the fluid velocity $\mathbf{v}$ at their current position and undergo a random diffusive step. We use an explicit Euler scheme to update the position $\mathbf{r}$ of each tracer molecule,

$$\mathbf{r}(t+\Delta t) = \mathbf{r}(t) + \mathbf{v}[\mathbf{r}(t)]\Delta t + \boldsymbol{\xi}(6D\Delta t)^{1/2}, \tag{5}$$

where $\boldsymbol{\xi}$ is a vector of unit length and random orientation. It may easily be shown that the concentration of many tracer molecules whose positions evolve according to such a Langevin equation satisfies the convection-diffusion equation, Eq. (4).[29] Many random steps of the form $\boldsymbol{\xi}(6D\Delta t)^{1/2}$ will lead to a Gaussian distributed probability of position for a tracer particle as expected for molecular diffusion. Choosing ξ from a Gaussian distribution would have the advantage of yielding a Gaussian displacement even after a single step but would lead in rare cases to very large displacements making the treatment of tracer-particle and tracer-wall collisions more complicated. The fluid velocity at the current tracer position is obtained by linear interpolation of the velocities obtained at the grid points of the lattice-Boltzmann simulation. The nodes within a solid particle were taken to have velocities given by the solid-body motion of the particle. For the nodes closest to the walls, quadratic interpolation of the velocity normal to the wall was implemented because the quadratic variation in the wall-normal velocity and linear variation in the wall-tangent velocity make comparable contributions to the mass flux in the boundary layer

near the wall.[30] During the simulation, both the tracer and solid particles are propagated in a given time step, and thereafter a test determines if the tracer has entered a solid particle due to its random displacement. In the event that it has entered the particle, a specular reflection is implemented which mimics the no flux boundary condition in the convection-diffusion equation. The reflection was performed at a boundary determined by the hydrodynamic radius of the solid particle. Tracers also undergo specular reflection from the solid walls. To simulate the reaction at the walls we keep track of two tracer particle species (A and B). All particles that reflect from one wall are converted to species A, while all particles that reflect from the other wall are converted to species B. This results in equal and opposite concentration driving forces for the two species of magnitude c_0 corresponding to the total number of tracers per unit fluid volume in the suspension. The appropriate thermodynamic driving force is the concentration per unit fluid volume which is equivalent to the chemical potential because the tracer concentration within the particles is zero at equilibrium with any fluid tracer concentration. This two-species method has the advantage that tracer particles need not be created or destroyed during the simulation. The concentration field of species A is equivalent to the field of species B reflected across the midplane (aside from statistical fluctuations). The mass transfer coefficient may be determined based on the flux of either species, and we used the average of the two fluxes to obtain better statistical accuracy.

The tracer method can be used at high values of the Peclet number for which the grid resolution for a finite difference solution of the convection-diffusion equation would need to be exceedingly fine. Because the concentration field is determined from a statistical average of the number of tracer particles in a test volume, the uncertainty in the detailed concentration field $c(x,y,z,t)$ would be large. Here, y is the spatial coordinate perpendicular to the walls. Fortunately, however, we will only require knowledge of the total mass flux $\langle Q \rangle$ (the number of A to B conversions at one of the walls per unit area per unit time) and the average concentration field $\langle c \rangle_f(y)$, where the angle brackets indicate an average over x, z, and t after the suspension has reached a statistical steady state and $\langle \ \rangle_f$ indicates an average over points within the fluid phase.

The simulations were performed in a unit cell with periodic boundary conditions in the x and z directions and solid boundaries in the y direction. The cell dimensions in the x and z directions were typically ten times the particle radius, while, for the gap thicknesses in the y direction, $H/a=10$, 15, and 20 were considered. The initial solid particle configuration was chosen from a hard-sphere distribution generated by a Monte Carlo routine and approximately 8000 tracer particles were placed with equal likelihood throughout the fluid. The walls were moved with velocities $\pm\Gamma H/2$ and the solid- and tracer-particle configurations subsequently evolved toward a statistical steady state. It was typically found that a total strain Γt of about 850 was required to achieve the steady state mass flux and concentration field. The results presented were then obtained as a time average over a subsequent period of $\Gamma t=850$. The statistical uncer-

tainty of the dimensionless mass transfer rate (Sherwood number), estimated as the standard deviation of the Sherwood numbers obtained during five subintervals, was typically 3%–7% of the mean value. The time step for the tracer calculation was $\Gamma \Delta t = 1.8 \times 10^{-3}$ and tests with a time step of about half this value increased the Sherwood number by less than 2%. Simulations using an x periodicity length of 15 times the particle radius increased the mass flux by 3%. Each of these changes was within the statistical uncertainty of the simulations. To test the adequacy of the grid resolution in a situation that was not subject to statistical uncertainty due to random particle configurations, we considered the steady flow produced by a single neutrally buoyant particle in the center of the gap with $H/a = 3.4$, Pe = 300, and Re = 0.5. The Sherwood number increased only from 1.47 to 1.48 and 1.49 as the sphere radius in lattice units was increased from $a = 2.92$ to $a = 5.04$ and $a = 8.46$. The lattice-Boltzmann simulations were performed with a fluid density of 36 and viscosity of 0.36 in lattice units. This relatively low viscosity allows one to access Reynolds numbers up to 10 while maintaining a small enough velocity in lattice units so that compressibility effects are small.

IV. RESULTS AND DISCUSSION

A. Mass transfer across a stationary suspension

A stationary suspension of impermeable particles will reduce the rate of mass transfer because the fluid-phase ions must diffuse around the solid particles. Maxwell[31] predicted the effective dielectric constant for a composite material consisting of a dilute dispersion of spheres in a matrix material with a different dielectric constant. This electrostatic problem is directly analogous to the problem of determining the effective thermal conductivity of a composite material. A good discussion of the analogy between heat and mass transfer is given by Deen,[32] and the mass transfer analog of the Maxwell theory is

$$\mathrm{Sh} = D_M^* = 1 + 3\phi \frac{\alpha - 1}{\alpha + 2}, \qquad (6)$$

where $\alpha = D_p M / D$, D_p and D are the diffusivities of the tracer in the particle and fluid phases, respectively, and M is the solubility ratio, defined as the ratio of the tracer concentration in the particle phase to that in the fluid phase when there is a local equilibrium at the particle surface. The Sherwood number given by Eq. (6) is equivalent to the ratio D_M^* of the effective diffusivity of the two-phase mixture, D_M, to the fluid-phase diffusivity D when the effective diffusivity is defined by considering a thermodynamic driving force equal to the mean fluid-phase concentration, i.e., $\langle Q \rangle = -D_M d\langle c \rangle_f / dy$.[32] This is expected to be a good approximation if the resistance of the layer within a distance of $O(a)$ of the wall where the suspension structure is influenced by the wall makes a small contribution to the overall mass transfer resistance. This is true when $\alpha \lesssim O(1)$ and $H/a \gg 1$. The Maxwell theory is strictly valid for $\phi \ll 1$. However, experiments[33] and numerical simulations[34] indicate that it remains a good approximation for ϕ as high as 0.6 when α is
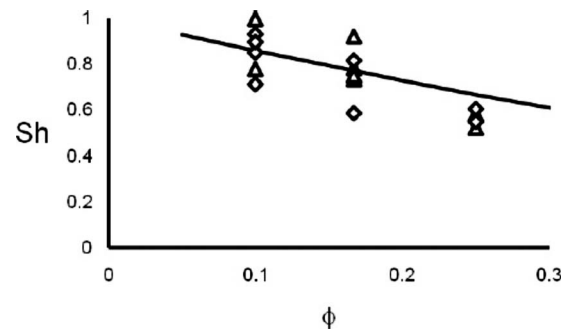

FIG. 1. The Sherwood number for mass transfer across a stationary suspension is plotted as a function of the particle volume fraction ϕ. The triangles and diamonds are experimental measurements with $H/a = 44$ and 22, respectively. The line is the Maxwell theoretical prediction, Eq. (6).

not too large. In our experiments, $M = 0$ so that $\alpha = 0$ and $D_M^* = 1 - 3\phi/2$.

The mass transfer rate in a stationary suspension was measured in the Couette cell. The experimental measurements of the mass transfer rate as a function of particle volume fraction are compared with the Maxwell prediction (line) in Fig. 1. The diamonds and squares are for $H/a = 22$ and 44, respectively. The results do not depend on H/a, suggesting that the resistance in the bulk of the suspension dominates. Despite some scatter, the results are in good agreement with the Maxwell prediction. This suggests that the particles were well dispersed and no significant sedimentation occurred and indeed the visual observation confirmed these suppositions.

B. Experimental measurements of mass transfer in a sheared suspension

We measured the rate of mass transfer in sheared suspensions with volume fractions $\phi = 0.1$, 0.17, and 0.25, ratios of the gap thickness to particle radius $H/a = 22$ and 44, and shear rates up to about 120 s^{-1} yielding Peclet numbers up to about 16 000 (4000) and Reynolds numbers up to about 6.6 (1.6) for the larger (smaller) particles. The experimental results for the mass transfer rate, Sh, as a function of the Peclet number for the $H/a = 22$ are plotted in Fig. 2. In the absence of particles (circles), there is a modest increase in Sh
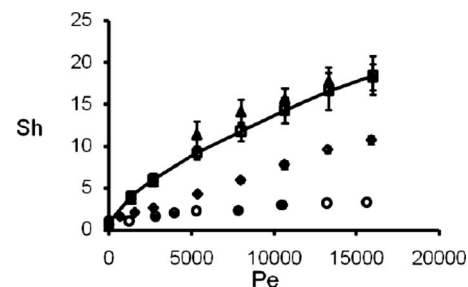

FIG. 2. Experimentally measured Sherwood number for mass transfer across sheared suspensions with $H/a = 22$ is plotted as a function of the Peclet number. Circles are measurements in the absence of particles. The diamonds, squares, and triangles are measurements in particle suspensions with $\phi = 0.1$, 0.17, and 0.25, respectively. The error bars are standard deviations of five experimental measurements, each made with a fresh suspension.
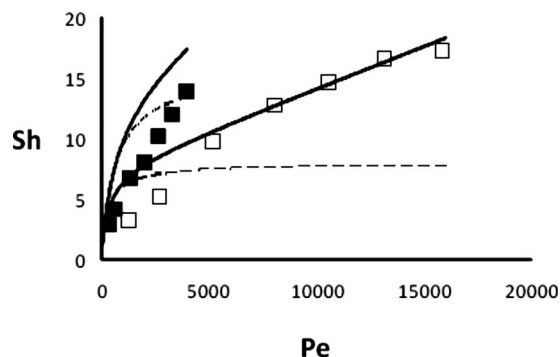
FIG. 3. Mass transfer rate as a function of Peclet number in suspensions with $\phi=0.17$. The filled and open squares are experimental measurements with $H/a=44$ and 22, respectively. The upper and lower solid lines are the theory, Eqs. (9), (11), and (12), for $H/a=44$ and 22, respectively. The dashed lines are the theoretical predictions neglecting the effects of fluid inertia, i.e., setting Re to zero in Eqs. (12) and (11).
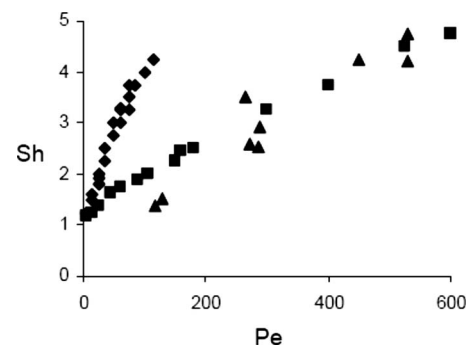

FIG. 4. The rate of mass transfer measured as a function of the Peclet number in sheared suspensions of polystyrene spheres with $\phi=0.15$ and $H/a=44$ in the present work (triangles) is compared with the mass transfer rate in a suspension of red-blood cells with $\phi=0.18$ and $H/a=110$ by Wang and Keller (Ref. 15) (diamonds) and the heat transfer rate in suspensions of polystyrene spheres in a viscous oil with $\phi=0.15$ and $H/a=18$ by Sohn and Chen (Ref. 16) (squares).

with shear rate. However, the enhancement of mass transfer in the presence of particles is much larger. The mass transfer rate increases with the Peclet number. The slope of the Sh versus Pe curve decreases with increasing Pe, rather than being constant as would be predicted if hydrodynamic diffusion dominated throughout the Couette gap. This suggests that molecular diffusion plays a greater role in mass transfer at higher shear rates. The mass transfer rate increases significantly as the particle volume fraction is increased from $\phi=0.1$ (diamonds) to 0.17 (squares). There is a further growth in Sh as ϕ is increased to 0.25 (triangles) that lies within the statistical uncertainty of the experiments. The error bars in Fig. 2 are the standard deviation among five experimental measurements taken with different particle suspensions prepared in the same manner. In Fig. 3, we compare the measurements for the small ($H/a=44$) and large ($H/a=22$) particles at the same volume fraction $\phi=0.17$. It can be seen that, after accounting for effects of the Peclet number and Reynolds number, the mass transfer rate is considerably larger when the particle size is smaller compared with the Couette gap thickness H. The smaller particles also exhibit a dependence of Sh on Pe that is closer to the linear relationship expected when hydrodynamic diffusion dominates. In the subsequent subsections we will interpret the dependence of the mass transfer rate Sh on the Peclet number, particle volume fraction, and gap-to-radius ratio using a simple analytical model with parameters that will be determined using numerical simulations.

The two previous experimental studies having the greatest similarity to the present investigation are a measurement of heat transfer through a system of polystyrene spheres suspended in a viscous oil[16] and an electrochemical measurement of mass transfer across a suspension of red-blood cells.[15] In both of these studies the suspensions were sheared in a cylindrical Couette cell and the transport was measured from one cylinder to the other as is done in the present work. We compare our measurements for $H/a=44$ and $\phi=0.17$ with Sohn and Chen's[16] heat transfer measurement for $H/a=18$ and $\phi=0.15$ and Wang and Keller's[15] mass transfer measurements for $H/a=110$ and $\phi=0.18$ in Fig. 4. For Wang

and Keller's measurements $a=4$ μm is the radius of the disklike red-blood cells. The previous measurements were performed for Re $\ll 1$ and the largest Reynolds number for our $H/a=44$ experiment is 1.6, so inertial effects are likely to have a small effect on this comparison. If Pe, ϕ, and H/a were the sole determinants of the mass transfer rate, we would expect our measured transport rates to be intermediate between those of Sohn and Chen and Wang and Keller. Instead, our measurements are closer to those conducted with a much smaller gap to particle size ratio by Sohn and Chen. We attribute this observation to the fact that the convective heat transport in Sohn and Chen's experiment would have been augmented by heat carried by the moving particles, whereas, in our experiments, the solid particles are impermeable to the chemical tracers. The ratio of the heat capacities per unit volume in the particle and fluid in Sohn and Chen's experiment was 0.82. The transport in Wang and Keller's experiment is also likely to be larger than that for a suspension of spheres with the same ϕ, Pe, and H/a because the disklike red-blood cells would produce a larger hydrodynamic disturbance per unit volume than spherical particles.

C. A simple theoretical model

In this subsection, we propose a simple theoretical model that accounts for the qualitative trends that we have noted in the dependence of mass transfer observed experimentally. The chaotic advection of fluid-phase tracers due to the hydrodynamic disturbances produced by the randomly distributed solid particles is expected to lead to an effective hydrodynamic diffusivity of the tracer D_H. At high Peclet numbers when the tracer particles' motion is dominated by advection, we postulate that the hydrodynamic diffusivity D_H is independent of the molecular diffusivity D. Far enough from the walls we may expect that this diffusivity will be independent of position and H/a. At low Re, dimensional analysis then implies that $D_H=\Gamma a^2 D_H^*$, where D_H^* is a dimensionless function of the volume fraction ϕ. We therefore assume that the flux across the channel is related to the average concentration in the bulk of the suspension far from the walls by

$$Q = -(D_H + D_M)\left(\frac{d\langle c \rangle_f}{dy}\right)_{\text{bulk}}.$$ (7)

Although hydrodynamic diffusion is expected to dominate at the relatively high Peclet numbers that predominate in our study, this formulation allows the mass transfer rate to pass smoothly over to the Maxwell result as Pe $\rightarrow 0$.

The no-slip boundary condition on the fluid velocity will decrease the amplitude of the random convective motions near the walls of the Couette flow leading to a reduction in the local hydrodynamic diffusivity. The depletion of particles near the wall due to wall-particle excluded volume may be expected to further decrease the hydrodynamic diffusion near the wall. The no-slip condition, in fact, implies that molecular diffusion must dominate within a boundary layer near each wall. One can expect a smooth transition between the hydrodynamic-diffusion dominated transport in the bulk suspension and the molecular-diffusion dominated transport near the wall. Lacking a detailed description of this transition, however, our model makes the simple approximation that the hydrodynamic diffusivity is zero within a boundary layer of thickness δ near each wall. Since the length scale of the random convective flow is the particle radius a, we postulate that $\delta^* = \delta/a$ is a dimensionless function of particle volume fraction ϕ. Within the boundary layer the flux is taken to be

$$Q = -D_M\left(\frac{d\langle c \rangle_f}{dy}\right)_{\text{bl}}.$$ (8)

Solving the model given by Eqs. (7) and (8) with the piecewise continuous concentration field and continuous mass flux that it implies yields

$$\frac{1}{\text{Sh}} = \frac{1 - 2\delta^*\left(\dfrac{a}{H}\right)}{\text{Pe } D_H^* + D_M^*} + \frac{2\delta^*\left(\dfrac{a}{H}\right)}{D_M^*}.$$ (9)

The first term on the right-hand side of Eq. (9) results from the mass transfer resistance of the bulk suspension, while the second term results from the resistance of the boundary layers at the two walls. The three mass transfer resistances are acting in series. This expression yields the qualitative trends observed in the experiments and provides a physical interpretation of these trends. For a bulk suspension $H/a \gg 1$ at moderately high values of the Peclet number $1 \ll \text{Pe} \ll H/a$, hydrodynamic diffusion is the predominant mass transfer resistance and Sh is proportional to Pe. As the Peclet number is further increased, however, the mass transfer resistance of the boundary layer becomes important and the rate of increase of mass transfer with Peclet number is diminished. Smaller particles (smaller a/H) fill the space near the planar walls with random flows more effectively than larger particles, yielding a thinner boundary layer with a smaller mass transfer resistance. Thus, Sh is larger for larger H/a at the same Pe and ϕ. Finally, if we suppose that the dimensionless hydrodynamic diffusivity of the fluid tracer, D_H^*, will be an increasing function of particle volume fraction (as is the case for solid particles[3]), then Sh will increase with increasing volume fraction.
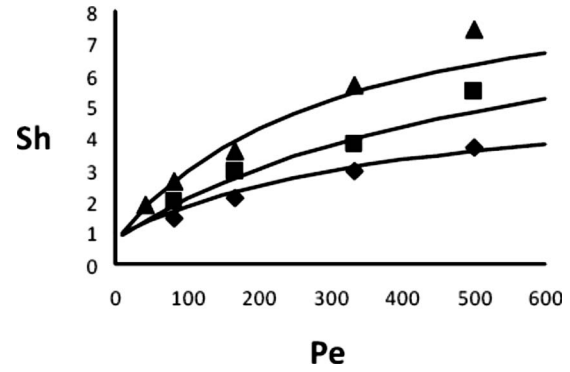

FIG. 5. The mass transfer rate obtained from the numerical simulations as a function of the Peclet number for $H/a = 20$ and several values of the particle volume fraction. The symbols indicate the transport rate obtained from the simulated mass flux to the wall. The lines are the theoretical model, Eq. (9), with the parameters listed in Table I which are obtained by fitting the mean concentration profile. The diamonds and bottom line are for $\phi = 0.1$, squares and middle line for $\phi = 0.17$, and triangles and top line for $\phi = 0.25$.

D. Numerical simulations of viscous suspensions

We performed a series of dynamic simulations of solid particle, fluid, and chemical tracer motion in viscous sheared suspensions to characterize the dependence of the mass transfer rate on the Peclet number Pe, particle volume fraction ϕ, and the gap-thickness-to-particle-radius ratio H/a. These simulations are computationally intensive owing to the need to gather adequate statistics for the mass transfer by following the motion of many tracer particles in a dynamically evolving flow field over a long period of dimensionless time Γt. Increasing Pe and/or H/a tends to increase the time required for the mass transfer process to reach equilibrium. Increasing H/a increases the number of fluid nodes. Decreasing Re increases the number of lattice-Boltzmann steps required for a given dimensionless time period. For these reasons our simulations were limited to a maximum Peclet number of 500, whereas the experiments involved Peclet numbers as large as 15 000. Nonetheless, we will see that the qualitative behavior of the mass transfer is similar in the simulations and experiments, and we will use the theoretical model to relate the simulation and experimental results. The largest gap thickness ratio accessible in the simulations $H/a = 20$ is comparable to the smaller gap thickness ratio $H/a = 22$ explored in the experiments. The viscous flow simulations were performed at a moderately low particle Reynolds number Re $= 0.5$ for which inertial effects on the mass transfer are expected to be modest. For example, at Pe $= 500$, $\phi = 0.17$, and $H/a = 10$, the Sherwood number increased only about 6% as the Reynolds number was increased from 0.5 to 1.5. Thus, we anticipate that the Re $= 0.5$ computational results for Sh are within about 3% of the low Re limiting values.

The simulation results for the Sherwood number are plotted as a function of the Peclet number in Fig. 5 for $H/a = 20$ and three different volume fractions $\phi = 0.1$ (diamonds), 0.17 (squares), and 0.25 (triangles). Figure 6 is a plot of Sh versus Pe for $\phi = 0.17$ and three values of the gap thickness $H/a = 10$ (diamonds), 15 (triangles) and 20 (squares). Comparing the simulation results in Figs. 5 and 6
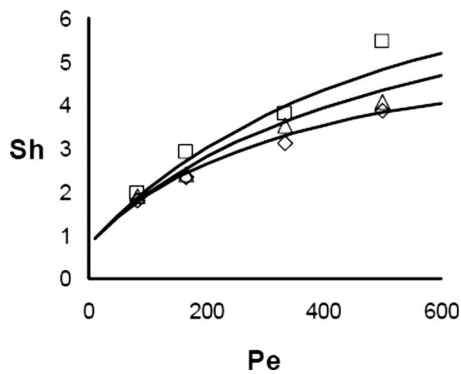
FIG. 6. The mass transfer rate obtained from the numerical simulations as a function of the Peclet number for $\phi=0.17$ and several values of the Couette-gap-to-particle-radius ratio. The symbols are obtained from the simulated mass flux to the wall. The lines are the theoretical model, Eq. (9), with the parameters listed in Table I which are obtained by fitting the mean concentration profile. The diamonds and bottom line are for $H/a=10$, triangles and middle line for $H/a=15$, and squares and top line for $H/a=20$.

with the experimental results in Figs. 2 and 3, it may be seen that all the qualitative trends of Sh with respect to Pe, ϕ, and H/a noted at the beginning of Sec. IV C are evident in the simulations as well as the experimental measurements.

In Sec. IV C, we introduced a model capable of explaining these trends in terms of parallel mass transfer resistances due to a hydrodynamic-diffusion-dominated bulk suspension and molecular-diffusion-dominated boundary layers at the bounding walls. The two parameters that appear in this model, the dimensionless hydrodynamic diffusivity D_H^* and dimensionless boundary layer thickness δ^*, could be determined by making a least-squares best fit of Eq. (9) to the simulation data for Sh as a function of Pe. However, a more direct determination of these parameters can be obtained using the concentration profile of the tracer molecules. Figure 7 illustrates the variation in the concentration of the tracer species produced at the wall at $y=0$ as a function of y/H for one
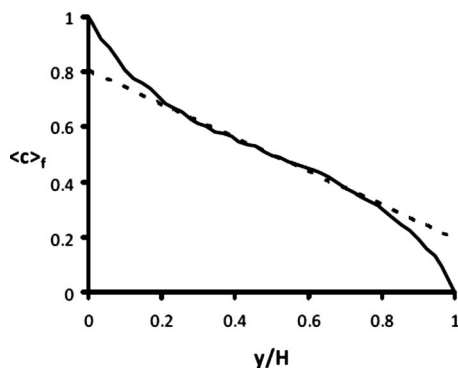

FIG. 7. A typical profile of the average concentration in the fluid phase obtained from the numerical simulations as a function of the distance y from one of the planar walls. The concentration is normalized by the concentration in equilibrium with the wall at $y=0$. The solid line is the fluid-phase concentration averaged over the xz plane and over time (after a statistical steady state is established). The dashed line is the best fit to the concentration profile in the middle third of the channel. The slope and intercept of this line are $(d\langle c\rangle_f/dy)_{\text{bulk}}$ and $1-\Delta\langle c\rangle_f$, which are used to determine the hydrodynamic diffusivity and boundary layer thickness. This profile corresponds to Pe=167, $\phi=0.17$, $H/a=20$, and Re=0.5 and exhibits a concentration slip $\Delta\langle c\rangle_f=0.20$.

typical simulation run. The concentration varies linearly with position across the bulk of the suspension where hydrodynamic diffusion dominates. The concentration gradient is larger near the wall where the convective transport is weaker and molecular diffusion plays a more important role. The hydrodynamic diffusivity D_H can be determined using $\langle Q\rangle=-(D_H+D_M)(d\langle c\rangle_f/dy)_{\text{bulk}}$, where $\langle Q\rangle$ is the simulated mass flux, D_M is the Maxwell diffusivity, and $(d\langle c\rangle_f/dy)_{\text{bulk}}$ is the slope of a best fit straight line to the simulation concentration profile in the middle third of the channel. Extrapolating this best fit straight line to $y/H=1$ yields a concentration slip $\Delta\langle c\rangle_f$ (By symmetry extrapolation to the other wall yields $1-\Delta\langle c\rangle_f$.) The boundary layer thickness δ may be obtained from the concentration slip using $\langle Q\rangle=D_M\Delta\langle c\rangle_f/\delta$.

The dimensionless hydrodynamic diffusivities and boundary layer thicknesses determined in this way showed no systematic variation with Peclet number over the range Pe=100–500. Therefore, we averaged the results from simulations at four Peclet numbers in this range and present the results for D_H^* and δ^* for various values of ϕ and H/a in Table I. The hydrodynamic diffusivity shows no statistically significant variation with H/a as we might expect for a bulk suspension property. The diffusivity increases with increasing solid particle volume fraction.

The value of the dimensionless hydrodynamic diffusivity inferred from our simulations for $H/a=20$ is consistent with previous experimental measurements of the hydrodynamic diffusivity of solid particles, although it should be noted that there is considerable statistical uncertainty in our values of D_H^* and considerable scatter among the previous measurements. Although there are no direct experimental measurements of the hydrodynamic diffusion of a chemical tracer in a bulk sheared suspension of solid particles, an indication of D_H^* can be obtained from experimental observations of the motion of small tracer solid spheres in suspensions of larger spheres. Breedveld et al.[7] performed such measurements with a particle size ratio of 0.1 in a suspension with a volume fraction of 0.3. Zarraga and Leighton observed a small sphere with a size ratio of 0.3 in a suspension with a volume fraction of 0.15. In both cases, the hydrodynamic diffusivity of the small tracer was found to be about 0.7 times the hydrodynamic diffusivity of the large solid particles. Our simulated value $D_H^*=0.033$ for a suspension with $\phi=0.25$ and $\phi_B=0.3$ is very close to the value $D_H^*=0.032$ measured by Breedveld et al. at $\phi_B=0.3$. In the most dilute suspension studied here, $\phi=0.1$ and $\phi_B=0.142$, we obtained $D_H^*=0.014$ which is somewhat higher than the measurement $D_H^*=0.0072$ of Zarraga and Leighton at $\phi_B=0.15$. Measurements of the hydrodynamic diffusivity of large solid particles at this volume fraction range from 0.009 to 0.016.[3,5]

The dependence of the solid-particle and fluid-tracer diffusivities on the particle volume fraction is complex. The streamlines for flow past a single neutrally buoyant particle in an unbounded simple shear flow have a fore-aft symmetry about the xz-plane, which implies that a nondiffusive fluid particle encountering a solid particle will return to its original y-position after the interaction. This implies that there is no $O(\phi)$ contribution to the hydrodynamic diffusivity and no

TABLE I. Numerical simulation results for suspension structure and mass-transfer-model parameters. The simulation conditions are characterized by the particle Reynolds number Re, the Couette-gap-to-particle-radius ratio H/a, and the nominal solid volume fraction ϕ. The mass transfer results are obtained from the mass flux and average concentration profiles and are averaged over four Peclet numbers in the range of $100 < \text{Pe} < 500$. The suspension structure is characterized by the bulk volume fraction averaged over the middle third of the channel, ϕ_B, and the thickness of a wall depletion layer normalized by the sphere radius, δ_D^*. The parameters appearing in the mass transfer model, Eq. (9), are the mass transfer boundary layer thickness normalized by the sphere radius δ^* and the hydrodynamic diffusivity D_H^*, which is normalized by Γa^2.

Re	H/a	ϕ	ϕ_B	δ_D^*	δ^*	D_H^*
0.5	10	0.1	0.169	2.05	1.06 ± 0.15	0.010 ± 0.003
0.5	15	0.1	0.143	2.25	1.43 ± 0.41	0.012 ± 0.002
0.5	20	0.1	0.142	2.94	1.52 ± 0.16	0.014 ± 0.005
4	20	0.1	0.0995	-0.05	0.70 ± 0.21	0.019 ± 0.002
0.5	10	0.17	0.245	1.54	0.66 ± 0.06	0.017 ± 0.003
0.5	15	0.17	0.225	1.84	0.74 ± 0.07	0.016 ± 0.003
0.5	20	0.17	0.220	2.28	0.83 ± 0.06	0.017 ± 0.002
4	20	0.17	0.175	0.29	0.54 ± 0.19	0.025 ± 0.005
0.5	10	0.25	0.301	0.85	0.65 ± 0.21	0.033 ± 0.007
0.5	15	0.25	0.302	1.30	0.63 ± 0.14	0.033 ± 0.002
0.5	20	0.25	0.302	1.73	0.71 ± 0.24	0.032 ± 0.004
4	20	0.25	0.274	0.88	0.46 ± 0.08	0.036 ± 0.005

$O(\text{Pe}\,\phi)$ contribution to the Sherwood number. Leal[35] considered the influence of isolated particles on mass transfer across a sheared suspension of diffusive fluid tracers for Pe $\ll 1$ and obtained a contribution to the Sherwood number that scaled as $\phi\,\text{Pe}^{1/2}$, while and Nir and Acrivos[36] showed that the corresponding contribution for Pe $\gg 1$ scaled as $\phi\,\text{Pe}^{1/11}$. It may be expected, however, that particles will produce a much larger rate of mass transfer at high Peclet number if there is any mechanism facilitating a net transport of particles in the y direction by purely hydrodynamic means. Leighton and Acrivos[3] originally proposed a correlation of their measured hydrodynamic diffusivities for solid particles that was proportional to ϕ^2. This ϕ^2 scaling reflects the idea that an encounter of a tracer solid (or fluid) particle with a pair of particles could produce a net y displacement. Leshansky and Brady's[9] simulations of solid particle hydrodynamic diffusion in periodic unit cells confirmed this scaling for the range $\phi = 0.05 - 0.15$. However, Zarraga and Leighton[5] measured hydrodynamic diffusivities of solid particles in a cylindrical Couette cell that were proportional to ϕ for $\phi < 0.1$. Recently, Zurita-Gotor *et al.*[6] have shown that the interaction of pairs of particles with a bounding wall can lead to a net displacement in the y direction and a hydrodynamic diffusivity that is proportional to ϕ and depends on H/a. Zarraga and Leighton's measurements begin to deviate from the ϕ-scaling when $\phi = 0.15$. Thus, it is likely that our most dilute suspension, for which $\phi_B = 0.14$, is in the transition region between a dilute suspension for which interactions of pairs of particles with the bounding wall control hydrodynamic diffusion and the concentrated regime in which many-particle interactions control hydrodynamic diffusion.

The boundary layer thickness is on the order of the particle radius $\delta^* = O(1)$. This is consistent with excluded volume depletion of particles from a region near the wall along with attenuation of hydrodynamic disturbances by the presence of the solid wall. The boundary layer is thicker for more

dilute suspensions and thinner in concentrated suspensions where more particle-particle interactions tend to push more particles toward the wall. For $\phi = 0.1$ and 0.17, there is some evidence for an increase in the boundary layer thickness as H/a is increased from 10 to 15. The further increase in δ^* as H/a is increased to 20 is less and is within the error bars. In our subsequent comparison with experimental results we will assume that the value of δ^* for $H/a = 20$ represents the large H/a limit.

In a previous study, Koch[11] proposed a model for mass transfer across a sheared suspension similar to Eq. (9), but with a boundary layer that became thinner as the Peclet number increased. In particular, Koch proposed $\delta = ka\,\text{Pe}^{-1/4}$, where k is a dimensionless parameter. We believe that Koch's model should be appropriate at asymptotically high Peclet numbers but that the Peclet numbers explored in the present study are not sufficiently high to make the previous model applicable. The hydrodynamic diffusivity of the tracer molecules should take on a constant value far from the bounding walls. It may then be expected to decrease as the distance y from the wall becomes $O(a)$. A qualitative sketch of this hydrodynamic diffusivity profile is given in Fig. 8. Koch[11] provided quantitative results for such a profile for the case of a wall-bounded fibrous porous medium for which the hydrodynamic diffusivity for arbitrary y can be evaluated analytically. For the case of a wall-bounded sheared suspension of neutrally buoyant particles, the fluid velocity disturbance tangent and normal to the wall due to the particles must be proportional to y and y^2, respectively, for $y/a \ll 1$ in order to satisfy the no-slip boundary condition and the continuity equation. The hydrodynamic diffusivity near the wall can be estimated as $D_H \sim \langle u_y'^2 \rangle \tau$, where $\langle u_y'^2 \rangle \sim \Gamma^2 y^4 / a^2$ is the normal component of the fluid velocity variance due to the particles and $\tau \sim 1/\Gamma$ is the time over which the fluid velocity disturbance seen by a tracer near the wall remains corre-
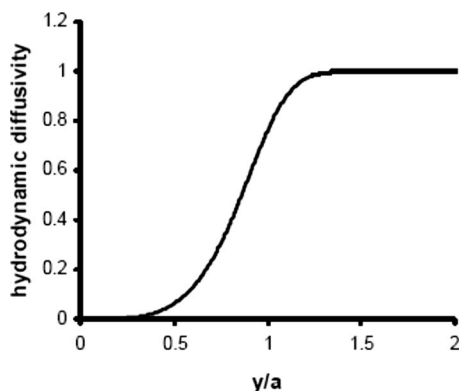
FIG. 8. Sketch of the profile of the hydrodynamic diffusivity as a function of distance from the planar wall normalized by the particle radius. The scaling of the wall-normal fluid velocity fluctuations inferred from the no-slip boundary condition and continuity imply that the diffusivity is proportional to y^4 as $y \to 0$. A profile that satisfies this constraint and approaches a constant as $y/a \to \infty$ is likely to have a very steep slope for a region where $y/a = O(1)$ so that there will exist a broad range of intermediate Pe for which the boundary layer thickness δ obtained by equating the hydrodynamic and molecular diffusivities is weakly dependent on Pe.

lated. These scalings imply that D_H should be proportional to $\Gamma y^4/a^2$ for $y \ll a$. If we determine the boundary layer thickness as the position at which the hydrodynamic and molecular diffusivities are equal, we obtain the scaling $\delta = ka \, \mathrm{Pe}^{-1/4}$ proposed by Koch.[11] However, from the constraints on D_H for small and large y, it is likely that the hydrodynamic diffusivity profile (Fig. 8) will have a region with a very steep slope when $y = O(a)$. Therefore, there would be a range of intermediate Pe values for which the value of δ determined by setting $D_H = D$ is relatively insensitive to Pe. We believe that the simulations and possibly also the experiments considered in this study lie within this intermediate range of Pe as all the evidence we have obtained is consistent with a boundary layer thickness that is independent of Pe.

The predictions of the theoretical model, Eq. (9), using the parameters obtained from the concentration profile and listed in Table I are compared with the simulation results for the Sherwood number in Figs. 5 and 6. The model predictions for the dependence of Sh on Pe are in good agreement with the simulated mass transfer rates, suggesting that the mass transfer rate is indeed determined by the coupled resistance of hydrodynamic diffusion in a bulk suspension and molecular diffusion in boundary layers.

E. Effects of inertia

Some of the experimental measurements were conducted for particle Reynolds numbers as high as 6.6. We were therefore interested in learning from numerical simulations what effect fluid and particle inertia may have on the rate of mass transfer. In a set of experiments with a single fluid and chemical tracer and therefore a single value of the Schmidt number ν/D, variation of the shear rate and/or particle radius simultaneously changes the Peclet number and Reynolds number. However, in a numerical simulation it is convenient to vary Re independently of Pe and thereby isolate the effects

on the mass transfer rate of the modification of the fluid velocity field (nondimensionalized by Γa) and solid particle configuration with increasing Re. The resulting insight can then be useful for interpreting the experimental results and differentiating the effects of inertia and convection on the increase in Sh with respect to Γ.

Before examining the simulation evidence, there are two conflicting arguments one might advance concerning the issue of whether fluid inertia tends to enhance or diminish the rate of mass transfer at a fixed Peclet number. First, one may expect that hydrodynamic disturbances produced by the particles decay less readily at finite Re so that the amplitude of the dimensionless fluid velocity fluctuations would be greater at higher Reynolds numbers. In addition, fluid inertia breaks the symmetry of the pairwise solid-solid and solid-tracer interactions allowing a net displacement of particles without requiring the influence of a third particle or bounding wall.[37,38] These effects may lead to an enhancement of the hydrodynamic diffusivity D_H^*. On the other hand, it is known that a single neutrally buoyant particle in a sheared fluid tends to migrate away from the wall at finite Reynolds numbers,[39–42] whereas a zero Re particle would maintain a constant y position as a result of the linearity of the equations of motion. If this migration of finite Reynolds number particles persists in a particle suspension and leads to a significant deficit of solid particles near the wall, it could result in smaller velocity fluctuations near the wall and a thicker molecular-diffusion-dominated boundary layer.

First, let us consider the evidence for inertial migration of single neutrally buoyant particles away from the walls of Couette flows from the previous literature and our own simulations. The migration of neutrally buoyant particles away from the walls of Couette cells was observed experimentally by Halow and Wills.[41,42] Vasseur and Cox[39] performed a perturbation analysis to determine the migration velocity of a particle away from the wall in a planar Couette flow in the limit of small Reynolds number. Their analysis assumed that the particle is far away from the wall, $y/a \gg 1$, allowing one to consider only the leading order multipoles in the analysis of the fluid velocity perturbations. They further assumed that fluid inertia acts as a small perturbation even on the length scale of the gap thickness; this condition requires $\mathrm{Re}_H = \mathrm{Re}(H/a)^2 \ll 1$. Feng and Joseph[40] performed finite element simulations of the migration of a circular particle in a two-dimensional planar Couette flow. Their results for the migration of circular particles for Re = 0.625 were found to be close to the asymptotic predictions of Vasseur and Cox for spherical particles, whereas their results for higher Re diverged from the theory. It should be noted, however, that this agreement could be fortuitous as there is no reason to believe that the rate of migration of a circular particle would be exactly the same as that of a spherical particle in the limit of small Reynolds number.

We performed lattice-Boltzmann simulations of the motion of a single spherical particle in a planar Couette flow with $H/a = 10$. The results of these simulations for Re = 0.1, 0.25, and 0.5 are compared with the theoretical predictions of Vasseur and Cox in Fig. 9. The theory predicts that the
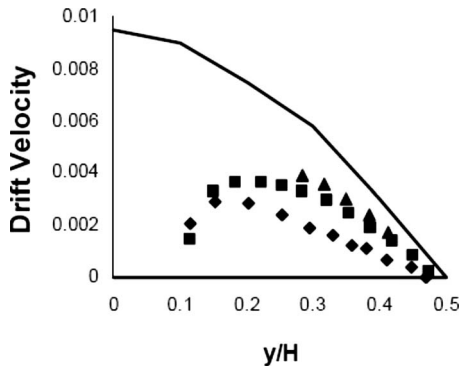
FIG. 9. Inertial migration of a single sphere in planar Couette flow. The wall-normal component of the velocity of a spherical particle normalized by ΓH Re is plotted as a function of the distance from the wall. The line is the asymptotic theory of Vasseur and Cox (Ref. 39) and the symbols are results of lattice-Boltzmann simulations with Re=0.5 (diamonds), 0.25 (squares), and 0.1 (triangles).

drift velocity normalized by ΓH Re will be a function of y/H for $\mathrm{Re}(H/a)^2 \ll 1$ and $y/a \gg 1$. Although our simulations do not strictly conform to the limits required by the theory, there is evidence that the migration velocity is approaching the theory for the range of positions $y/H=0.25-0.45$ as the Reynolds number is decreased from Re=0.5 to 0.25 and 0.1. Within this range, the velocity decreases with increasing y/H in a manner consistent with the theory and the normalized drift velocity $U_y/(\Gamma H \, \mathrm{Re})$ (where U_y is the y component of the particle velocity) is approaching the theoretical prediction with decreasing Re. In the range $y/H=0.1-0.25$ corresponding to $(y-a)/a=0-1.5$, the near-wall hydrodynamic interactions retard the migration of the particle away from the wall. The simulation velocity approaches zero as $(y-a)/a \to 0$ due to lubrication interactions, whereas these interactions are not incorporated in the theory. The simulation results approach zero before the particle reaches the precise center of the channel, and we believe that this is an artifact of the lattice. When the tendency for migration is small, it is possible that variations in the particle's position relative to the lattice can artificially stop its motion. Nonetheless, Fig. 9 indicates that a single particle in our lattice-Boltzmann simulation exhibits inertial migration away from the Couette walls in a manner consistent with the previous theoretical literature.

While a single particle in a planar Couette flow will migrate steadily toward the center plane, the convective flux of particles due to inertial migration in a particle suspension may be opposed by a flux due to hydrodynamic solid-particle diffusion leading to a relatively homogeneous particle suspension. This indeed seems to be the case in our simulations. In all the particle suspension simulations performed, we found a nearly homogeneous particle volume fraction in the center of the Couette gap with a slight depletion at the walls caused by excluded volume interactions and inertial migration. A simple way to quantify this depletion is to define a depletion length for the particle configuration δ_D. We determined the bulk volume fraction ϕ_B as the average fraction of the volume of the central one-third of the Couette gap that is filled with solid. If we then idealized the volume fraction
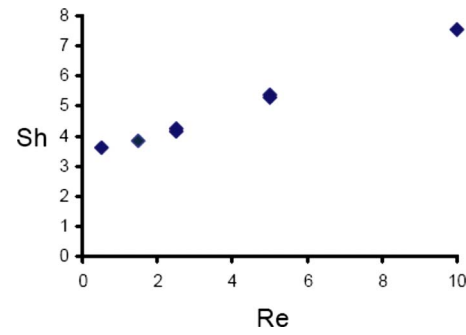

FIG. 10. (Color online) The mass transfer rate obtained from numerical simulations is plotted as a function of particle Reynolds number at a fixed value of the Peclet number Pe=500, ϕ=0.17, and H/a=10.

profile as consisting of a region of constant volume fraction ϕ_B that fills the region $\delta_D < y < H - \delta_D$ and regions of zero volume fraction for $0 < y < \delta_D$ and $H - \delta_D < y < H$, then we can determine the depletion layer thickness as

$$\delta_D = \frac{H}{2}\left(1 - \frac{\phi}{\phi_B}\right), \tag{10}$$

where ϕ is the nominal volume fraction defined as the fraction of the total Couette gap filled with solid. In Table I, we present simulation results for the nondimensional depletion layer thickness $\delta_D^* = \delta_D/a$. The depletion layer thickness is about one to three particle radii at Re=0.5 and it decreases with increasing particle volume fraction as may be expected if particle-particle interactions tend to push particles back toward the wall. We found that a calculation based on a model that balances the convective flux due to the inertial migration predicted by Vasseur and Cox[39] with a hydrodynamic diffusion flux estimated using results of Leighton and Acrivos[3] predicted that hydrodynamic diffusion is indeed strong enough to maintain a nearly uniform particle volume fraction across the gap except for regions close to the wall.[43] The predictive value of this model was limited, however, because the predicted migration velocity and measured hydrodynamic diffusivity are only known in the limit of small Reynolds numbers. At a higher Reynolds number, Re=4, we found that the depletion layer thickness was actually reduced relative to that found at Re=0.5. This may be a result of the more intense velocity fluctuations of both the fluid and solid particles in the presence of substantial inertial effects.

The depletion of particles near the wall did not lead to large perturbations in the mean fluid and particle velocity profiles (fluid velocity averaged over x and z positions and time). In all the simulations the average flow was very close to a simple shear flow in the bulk of the suspension. Fitting the average velocity in the bulk suspension with a linear function of y and extrapolating this line to $y=0$ indicated a slip velocity which never exceeded 3% of the wall velocity.

The results of a series of simulations to probe the dependence of the mass transfer rate on the Reynolds number are presented in Fig. 10. For this series of simulations we kept the Peclet number fixed at 500, ϕ=0.17 and H/a=10. The Sherwood number exhibits a nearly linear growth with Re increasing from Sh=3.6 at Re=0.5 to Sh=7.5 at Re=10. We
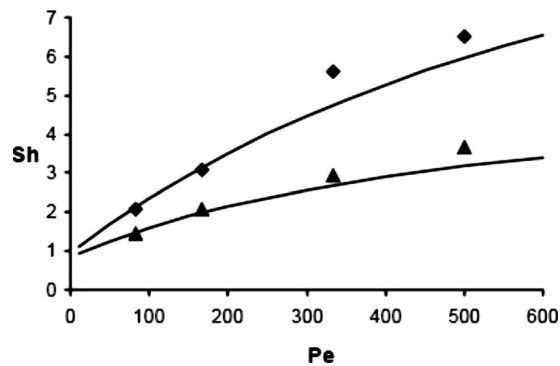
FIG. 11. The simulated mass transfer rate is plotted as a function of the Peclet number for two values of the particle Reynolds number: for the lower line and triangles Re=0.5 and for the upper line and diamonds Re=4. The symbols are obtained from the simulated mass flux to the wall. The lines are the theoretical model, Eq. (9), with the parameters listed in Table I which are obtained by fitting the mean concentration profile. The solid particle volume fraction is 0.1 and H/a=20.

FIG. 12. The mass transfer rate is plotted as a function of the Peclet number for H/a=44. The symbols are experimental measurements and the lines are the theoretical model, Eqs. (9), (11), and (12), with the parameters determined solely from the numerical simulations. The diamonds and lowest line are for ϕ=0.1, squares and middle line for ϕ=0.17, and triangles and highest line for ϕ=0.25.

therefore conclude that the enhanced mixing effect of a finite Reynolds number flow facilitates increased mass transfer with increasing Reynolds number.

We conducted mass transfer simulations with the largest gap thickness H/a=20 for Re=4 and the three volume fractions considered in the study ϕ=0.1, 0.17, and 0.25. The results for the hydrodynamic diffusivity and boundary layer thickness are listed in Table I. The hydrodynamic diffusivity grows with increasing Reynolds number as might be expected if inertia enhances the agitation of the system. The molecular-diffusion boundary layer thickness decreases when Re is increased from 0.5 to 4 consistent with the decreased particle depletion layer thickness.

Figure 11 shows simulation results and model predictions for the mass transfer rate Sh as a function of the Peclet number in a suspension with ϕ=0.1 and H/a=20 at two values of the Reynolds number Re=0.5 and Re=4. The dependence of the mass transfer rate on Peclet number is qualitatively similar at the two Reynolds number but the magnitude of the Sherwood number is larger at the larger Reynolds number. The theoretical model is in good agreement with the simulated mass transfer rate at both values of Re.

F. Comparison of model predictions with experiments

We will now compare the predictions of the theoretical model [Eq. (9)] with parameters D_H^* and δ^* determined from numerical simulations to the experimental mass transfer measurements. To mitigate the uncertainties that come from the determination of D_H^* and δ^* in individual simulation runs and to provide a general theoretical model, we will propose an analytical fit to the dependence of these parameters on ϕ and Re. Since the mass transfer rate was found to have a linear dependence on Re at a fixed Pe and H/a (see Fig. 10), we will assume that D_H^* and $1/\delta^*$ are linearly related to Re. Based on the simulation results given in Table I, we choose to fit $1/\delta^*$ and D_H^* as linear functions of ϕ,

$$D_H^* = (0.118 + 0.008\,\mathrm{Re})\phi \qquad (11)$$

and

$$\frac{1}{\delta^*} = 0.21(1 + 21.2\phi)(1 + 0.21\,\mathrm{Re}), \qquad (12)$$

where the numerical coefficients are determined from a least-squares best fit to the simulation data for H/a=20 in Table I.

The theoretical model, Eqs. (9), (11), and (12), is compared with the experimental measurements for the mass transfer rate as a function of Peclet number for the small particles, H/a=44, in Fig. 12 and for the large particles, H/a=22, in Fig. 13. The theoretical model is also presented in Fig. 3 where one can better see the nature of the predicted dependence of Sh on H/a. The model predicts all the qualitative features observed in the experiments. The Sherwood number increases linearly with Pe at moderate Pe due to the resistance caused by hydrodynamic diffusion in the bulk suspension but increases more slowly at higher Pe when the boundary layer mass transfer resistance is more important.

In the experimental study, Pe and Re vary simultaneously because the Schmidt number Sc=ν/D=Pe/Re is held fixed. It is worth noting that the gradual growth of the
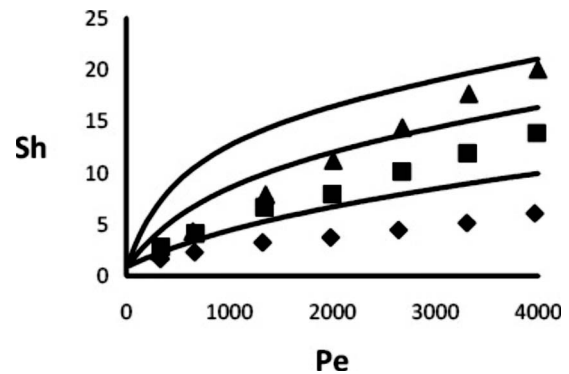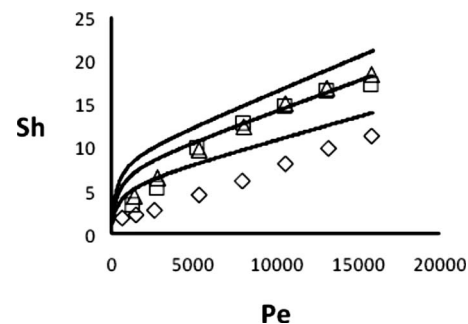

FIG. 13. The mass transfer rate is plotted as a function of the Peclet number for H/a=22. The symbols are experimental measurements and the lines are the theoretical model, Eqs. (9), (11), and (12), with the parameters determined solely from the numerical simulations. The diamonds and lowest lines are for ϕ=0.1, squares and middle line for ϕ=0.17, and triangles and highest line for ϕ=0.25.

mass transfer rate with increasing shear rate evident in the model predictions for $H/a=22$ at the highest shear rates results from the effects of fluid inertia. The dashed lines in Fig. 3 are the model predictions that would be obtained using the small Re limit of the theory, while allowing the Pe in the theory to match that in the experiments. It can be seen by comparing the dashed and solid lines in Fig. 3 that the continued increase in mass transfer with increasing shear rate for the larger particles is caused by the enhanced mixing due to fluid inertia.

The theory and experiment show comparable increases in mass transfer with increasing particle volume fraction. In the model this effect results from both the enhancement of the hydrodynamic diffusivity and the diminution of the boundary layer thickness with increasing ϕ. The theory accounts well for the increased rate of mass transfer for a given Pe as the ratio of the gap thickness to the particle radius H/a is increased. This constitutes an important test of the hypothesis of coupled hydrodynamic and boundary layer resistances. The smaller particles more efficiently fill the gap with chaotic fluid motion even at small distances from the wall, leading to a smaller boundary layer thickness.

V. CONCLUSION

We have presented a model for mass transfer across a sheared suspension of neutrally buoyant spheres. The transport results from the coupled effects of hydrodynamic diffusion in the bulk suspension and molecular diffusion in boundary layers near the two walls of the Couette flow. The parameters of the model, hydrodynamic diffusivity and boundary layer thickness, were obtained from numerical simulations based on the lattice-Boltzmann method for the fluid and solid particle motions and a tracer algorithm for the chemical species transport. Values of the hydrodynamic diffusivity of the chemical tracers derived from the simulations were consistent with experimental measurements[5,7] for small solid particles interacting with larger particles. This model predicted the qualitative trends of the mass transfer rate with Peclet number, Couette-gap-to-sphere-radius ratio H/a, and volume fraction observed in our experimental study of the transport of ferrocyanide ions through a density-matched suspension of polystyrene spheres. The mass transfer rate grows relatively rapidly with increasing Pe when the Peclet number is moderately large $1 \ll \text{Pe} \ll H/a$ and this growth can be attributed to the effects of hydrodynamic diffusion in the bulk suspension. As the Peclet number is further increased, however, the mass transfer resistance becomes increasingly dominated by the molecular-diffusion boundary layer. In the absence of fluid inertia, the model would predict a constant rate of mass transfer at high Peclet number. However, the increased agitation due to fluid inertia allows the mass transfer rate to continue to grow, albeit at a lower rate, when Pe is very large and $\text{Re} = O(1-7)$. The mass transfer rate increases with increasing volume fraction as a result of both the increased hydrodynamic diffusivity and the decreased boundary layer thickness.

[1] S. A. Khan, A. Guenther, M. A. Schmidt, and K. F. Jensen, "Microfluidic synthesis of colloidal silica," Langmuir **20**, 8604 (2004).

[2] W. J. Federspiel and R. G. Svitek, in *Encyclopedia of Biomaterials and Biomedical Engineering*, edited by G. E. Wnek and G. L. Bowlin (Dekker, New York, 2004), p. 922.

[3] D. Leighton and A. Acrivos, "Measurement of shear-induced self-diffusion in concentrated suspension of spheres," J. Fluid Mech. **177**, 109 (1987).

[4] D. R. Foss and J. F. Brady, "Self-diffusion in sheared suspensions by dynamic simulation," J. Fluid Mech. **401**, 243 (1999).

[5] I. E. Zarraga and D. T. Leighton, "Measurement of an unexpectedly large shear-induced self-diffusivity in a dilute suspension of spheres," Phys. Fluids **14**, 2194 (2002).

[6] M. Zurita-Gotor, J. Blawzdziewicz, and E. Wajnryb, "Swapping trajectories: A new wall-induced cross-streamline particle migration mechanism in a dilute suspension of spheres," J. Fluid Mech. **592**, 447 (2007).

[7] V. Breedveld, D. van den Ende, A. Tripathi, and A. Acrivos, "The measurement of the shear-induced particle and fluid tracer diffusivities in concentrated suspensions by a novel method," J. Fluid Mech. **375**, 297 (1998).

[8] Y. Wang, R. Mauri, and A. Acrivos, "The transverse shear-induced liquid and particle tracer diffusivities of a dilute suspension of spheres undergoing a simple shear flow," J. Fluid Mech. **327**, 255 (1996).

[9] A. M. Leshansky and J. F. Brady, "Dynamic structure factor study of diffusion in strongly sheared suspensions," J. Fluid Mech. **527**, 141 (2005).

[10] A. Sierou and J. F. Brady, "Shear-induced self-diffusion in non-colloidal suspensions," J. Fluid Mech. **506**, 285 (2004).

[11] D. L. Koch, "Hydrodynamic diffusion near solid boundaries with applications to heat and mass transport into sheared suspensions and fixed fiber beds," J. Fluid Mech. **318**, 31 (1996).

[12] A. J. C. Ladd, "Numerical simulations of particulate suspensions via a discretized Boltzmann equation. Part 1: Theoretical foundations," J. Fluid Mech. **271**, 285 (1994).

[13] A. J. C. Ladd, "Numerical simulations of particulate suspensions via a discretized Boltzmann equation. Part 2: Numerical results," J. Fluid Mech. **271**, 311 (1994).

[14] A. J. C. Ladd and R. Verberg, "Lattice-Boltzmann simulations of particle-fluid suspensions," J. Stat. Phys. **104**, 1191 (2001).

[15] N. L. Wang and K. H. Keller, "Augmented transport of extracellular solutes in concentrated erythrocyte suspensions in Couette flow," J. Colloid Interface Sci. **103**, 210 (1985).

[16] C. W. Sohn and M. M. Chen, "Microconvective thermal conductivity in disperse two-phase mixtures as observed in a low velocity Couette flow experiment," ASME Trans. J. Heat Transfer **103**, 47 (1981).

[17] X. Chen and M. Louge, "Heat transfer enhancement in dense suspensions of agitated solids. Part 1. Theory," Int. J. Heat Mass Transfer **51**, 5108 (2008).

[18] X. Chen and M. Louge, "Heat transfer enhancement in dense suspensions of agitated solids. Part 2. Experiments in the exchange limit," Int. J. Heat Mass Transfer **51**, 5119 (2008).

[19] J. R. Selman and C. W. Tobias, "Mass-transfer measurements by the limiting-current technique," Adv. Chem. Eng. **10**, 211 (1978).

[20] J. R. Selman and J. C. McClure, "Limiting current to a vertical rotating rod electrode," J. Electroanal. Chem. **110**, 79 (1980).

[21] D. W. Gibbons, R. H. Muller, and C. W. Tobias, "Mass transport to cylindrical electrodes rotating in suspensions of inert microspheres," J. Electrochem. Soc. **138**, 3255 (1991).

[22] E. F. C. Somerscales and M. Kassemi, "Electrochemical mass-transfer studies in open cavities," J. Appl. Electrochem. **15**, 405 (1985).

[23] R. J. Goldstein, V. Khan, and V. Srinivasan, "Mass transfer from inclined cylinders at moderate Rayleigh number including the effects of end face boundary conditions," Exp. Therm. Fluid Sci. **31**, 741 (2007).

[24] A. J. Arvia, S. L. Marchiano, and J. J. Podesta, "Diffusion of ferrocyanide and ferricyanide ions in aqueous solutions of potassium hydroxide," Electrochim. Acta **12**, 259 (1967).

[25] H. Schlichting, *Boundary Layer Theory* (McGraw-Hill, New York, 1955), p. 357.

[26] J.-P. Matas, J. F. Morris, and E. Guazzelli, "Influence of particles on the transition to turbulence in pipe flow," Philos. Trans. R. Soc. London, Ser. A **361**, 911 (2003).

[27] A. S. Sangani and A. Acrivos, "Slow flow through a periodic array of spheres," Int. J. Multiphase Flow **8**, 343 (1982).

[28] X. Yin and D. L. Koch, "Hindered settling velocity and microstructure in suspensions of spheres with moderate Reynolds number," Phys. Fluids **19**, 093302 (2007).

[29] W. B. Russel, D. A. Saville, and W. R. Schowalter, *Colloidal Dispersions* (Cambridge University Press, Cambridge, 1989), p. 69.

[30] L. G. Leal, *Laminar Flow and Convective Transport Processes* (Butterworth-Heineman, Boston, 1992).

[31] J. C. Maxwell, *Electricity and Magnetism* (Clarendon, Oxford, 1892), Vol. 1.

[32] W. M. Deen, *Analysis of Transport Phenomena* (Oxford University Press, Oxford, 1998), pp. 192–194.

[33] J. C. R. Turner, "Two phase conductivity: The electrical conductance of liquid-fluidized beds of spheres," Chem. Eng. Sci. **31**, 487 (1976).

[34] R. T. Bonnecaze and J. F. Brady, "The effective conductivity of random suspensions of spherical particles," Proc. R. Soc. London, Ser. A **432**, 445 (1991).

[35] L. G. Leal, "On the effective conductivity of a dilute suspension of spherical drops in the limit of low particle Peclet number," Chem. Eng. Commun. **1**, 21 (1973).

[36] A. Nir and A. Acrivos, "Effective thermal conductivity of sheared suspensions," J. Fluid Mech. **78**, 33 (1976).

[37] P. M. Kulkarni and J. F. Morris, "Pair-sphere trajectories in finite-Reynolds-number shear flow," J. Fluid Mech. **596**, 413 (2008).

[38] G. Subramanian and D. L. Koch, "Inertial effects on the transfer of heat or mass from neutrally buoyant spheres in linear velocity fields," Phys. Fluids **18**, 073302 (2006).

[39] P. Vasseur and R. G. Cox, "The lateral migration of a spherical particle in a two-dimensional shear flow," J. Fluid Mech. **78**, 385 (1976).

[40] J. Feng, H. H. Hu, and D. D. Joseph, "Direct simulation of initial value problems for the motion of solid bodies in a Newtonian fluid. Part 2. Couette and Poiseuille flows," J. Fluid Mech. **277**, 271 (1994).

[41] J. S. Halow and G. B. Wills, "Radial migration of spherical particles in Couette systems," AIChE J. **16**, 281 (1970).

[42] J. S. Halow and G. B. Wills, "Experimental observations of sphere migration in Couette systems," Ind. Eng. Chem. Fundam. **9**, 603 (1970).

[43] L. Wang, "Mass transfer in sheared suspensions of neutrally buoyant particles: Hydrodynamic diffusion across a suspension and inertial effects on interphase mass transfer," Ph.D. thesis, Cornell University, 2008.